Electron Mobility and Injection Dynamics in Mesoporous ZnO, SnO_2, and TiO_2 Films Used in Dye-Sensitized Solar Cells

Priti Tiwana, Pablo Docampo, Michael B. Johnston, Henry J. Snaith,* and Laura M. Herz*

Department of Physics, Clarendon Laboratory, University of Oxford, Parks Road, Oxford, OX1 3PU, United Kingdom

ABSTRACT High-performance dye-sensitized solar cells are usually fabricated using nanostructured TiO_2 as a thin-film electron-collecting material. However, alternative metal-oxides are currently being explored that may offer advantages through ease of processing, higher electron mobility, or interface band energetics. We present here a comparative study of electron mobility and injection dynamics in thin films of TiO_2, ZnO, and SnO_2 nanoparticles sensitized with Z907 ruthenium dye. Using time-resolved terahertz photoconductivity measurements, we show that, for ZnO and SnO_2 nanoporous films, electron injection from the sensitizer has substantial slow components lasting over tens to hundreds of picoseconds, while for TiO_2, the process is predominantly concluded within a few picoseconds. These results correlate well with the overall electron injection efficiencies we determine from photovoltaic cells fabricated from identical nanoporous films, suggesting that such slow components limit the overall photocurrent generated by the solar cell. We conclude that these injection dynamics are not substantially influenced by bulk energy level offsets but rather by the local environment of the dye—nanoparticle interface that is governed by dye binding modes and densities of states available for injection, both of which may vary from site to site. In addition, we have extracted the electron mobility in the three nanoporous metal-oxide films at early time after excitation from terahertz conductivity measurements and compared these with the time-averaged, long-range mobility determined for devices based on identical films. Comparison with established values for single-crystal Hall mobilities of the three materials shows that, while electron mobility values for nanoporous TiO_2 films are approaching theoretical maximum values, both early time, short distance and interparticle electron mobility in nanoporous ZnO or SnO_2 films offer considerable scope for improvement.

KEYWORDS: dye-sensitized solar cells · metal-oxides · nanoporous films · terahertz spectroscopy · charge injection · electron mobility · TiO_2 · ZnO · SnO_2

Over the past two decades, dye-sensitized solar cells (DSCs) with the highest performance have generally been those fabricated using TiO_2 nanoporous films as the electron-transporting electrode.[1] However, a significant amount of effort is currently being invested into trying to find alternative metal-oxides, such as SnO_2, ZnO, Nb_2O_5, and WO_3,[2−6] that may offer additional advantages in terms of device fabrication and characteristics. ZnO and SnO_2 are two particularly promising candidates because the electron mobility in their bulk single-crystal phases[7−10] is over 2 orders of magnitude higher than that for TiO_2.[11] As a result, it should also be possible to achieve higher overall electron mobility in the respective nanostructured films of ZnO and SnO_2, which may in turn minimize interfacial charge recombination losses to oxidized redox species in the electrolyte or solid-state hole transporter, thus improving device performance.

For comparison, the conduction band (CB) and valence band (VB) energies of TiO_2, ZnO, and SnO_2[2−5,12,13] are illustrated schematically in Figure 1. The band gap of ZnO is similar to that of TiO_2 at 3.2 eV, while SnO_2 displays a significantly larger band gap of 3.8 eV. As a result, SnO_2 is less likely to generate holes in the VB through direct photon absorption, and devices based on the material ought to be more robust under UV illumination than those made from TiO_2 or ZnO. In addition, the CB edge of SnO_2 is about 500 mV more positive than that of TiO_2, thus suggesting that charge injection in SnO_2-based DSCs could be faster than in their TiO_2 counterparts, even though at the cost of lower open-circuit device voltage (V_{OC}).

Despite the apparent advantages of ZnO and SnO_2, photovoltaic cells based on thin nanostructured films incorporating these materials have so far failed to overtake the best TiO_2-based devices in terms of performance. In order to examine the reasons for this discrepancy, we have conducted a combined study correlating the terahertz conductivity dynamics of dye-sensitized thin films made of sintered pastes of TiO_2, ZnO, and SnO_2 nanoparticles, with the properties of photovoltaic cells incorporating identical films. Optical pump terahertz probe (OPTP) spectroscopy is a highly useful

* Address correspondence to h.snaith@physics.ox.ac.uk, l.herz@physics.ox.ac.uk.

Received for review April 4, 2011 and accepted May 19, 2011.

Published online May 19, 2011
10.1021/nn201243y

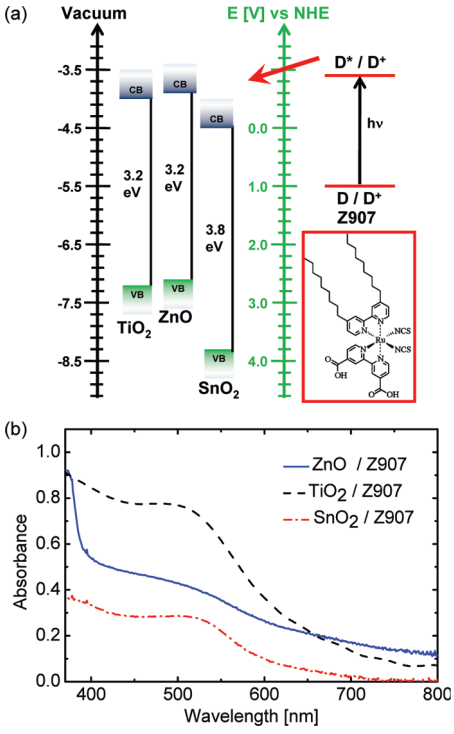

Figure 1. (a) Schematic diagram illustrating the energy levels of the conduction band (CB) and valence band (VB) of TiO_2, ZnO, and SnO_2 as taken from refs 2−5. Also shown is the approximate redox potential of ground and excited states of Z907 ruthenium-based dye[18] (molecular structure shown in inset). The red arrow indicates electron injection from the dye LUMO states into the respective metal-oxide CB. (b) Steady-state absorption spectra measured for sensitized nanoporous films of ZnO (blue solid line, film thickness 0.6 μm), SnO_2 (red dash-dot line, film thickness 1 μm), and TiO_2 (black dashed line, film thickness 3 μm) using an integrating sphere. Spectra were taken for film samples used in the terahertz photoconductivity measurements, and these data were used to calculate the terahertz effective mobility $\phi_{inj}\mu_{THz}$. We note that the films used for the solar cells below are much thicker and therefore display a higher optical density (OD > 2) at the absorption maximum. Details of film preparation and thicknesses are given in the Materials and Methods section.

technique allowing measurement of the charge conductivity of a medium with subpicosecond time resolution.[14,15] As an all-optical technique, it avoids issues arising from the possible existence of non-Ohmic contacts and hence yields charge mobility values directly attributable to the properties of the embedded active material. In addition, for dye-sensitized metal-oxide nanoporous films, OPTP allows the direct observation of time-dependent charge injection in the dye/semiconductor system,[4,16] without the need for complex analysis of multiple overlapping signals of different origins that often arise with more common measurement techniques, such as transient absorption spectroscopy.[17]

Our investigations show that, for ZnO and SnO_2 nanoporous films, electron injection from the sensitizer contains significantly slow (~tens to hundreds of picoseconds) components that are correlated with lowered injection efficiencies determined for corresponding devices. In contrast, for TiO_2, the injection efficiency is found to be near-unity. In addition, we demonstrate that while terahertz and device electron mobility values for nanoporous TiO_2 films approach theoretical maximum values, for ZnO and SnO_2 both early time, short-distance and long-range, interparticle electron mobility could be improved by several orders of magnitude.

RESULTS AND DISCUSSION

Figure 2 shows the OPTP normalized conductivity curves for the three dye-sensitized metal-oxide nanoporous films as a function of time after excitation of the Z907 dye. All three metal-oxide materials have sufficiently large band gaps (see Figure 1) in order for the VIS excitation pulses to generate excitations almost solely on the dye sensitizers.[16] The measured photoconductivity signal originates from mobile electrons subsequently injected into the metal-oxide films since, in comparison, the remaining holes on the dye molecules are essentially stationary. Such measurements allow an investigation of both the dynamics of the conductivity and the initial electron mobility achieved in the material.[16] In the first part of this discussion, we will focus on analyzing the electron injection dynamics and then proceed in the second part to examine the achieved terahertz mobility and compare it to bulk and device mobilities.

Multiphasic electron injection dynamics are displayed by all three metal-oxide films, with an initial fast injection component followed by slow rise phases, albeit with different weightings. In order to quantify the components contributing to the conductivity dynamics of electrons in the CBs or the metal-oxides, we have fitted the sum of three exponentials to the curves, as displayed in Figure 2, together with the data. Table 1 shows the time constants and weightings extracted from these fits. Remarkably, all three systems display a fast component with rise time of ~1 ps followed by a slower electron injection phase with time constants of a few tens of picoseconds. Overall, electron injection from Z907 into TiO_2 evidently proceeds fastest, followed by that into SnO_2, while ZnO shows the slowest overall injection rate.

Multiphasic charge injection involving slow delayed components has been previously reported for dye-sensitized ZnO,[4,5,19−22] TiO_2,[16,23−26] and SnO_2[4,5,17,27,28] studied by various experimental techniques such as ultrafast transient absorption spectroscopy,[19,20] mid-IR probe,[4,21,22] and microwave[5] or terahertz[16] conductivity measurements. However, absolute rise times reported even for the same metal-oxide material vary substantially between the different studies. These discrepancies should not be surprising since these studies involved films made with nanoparticles of varying

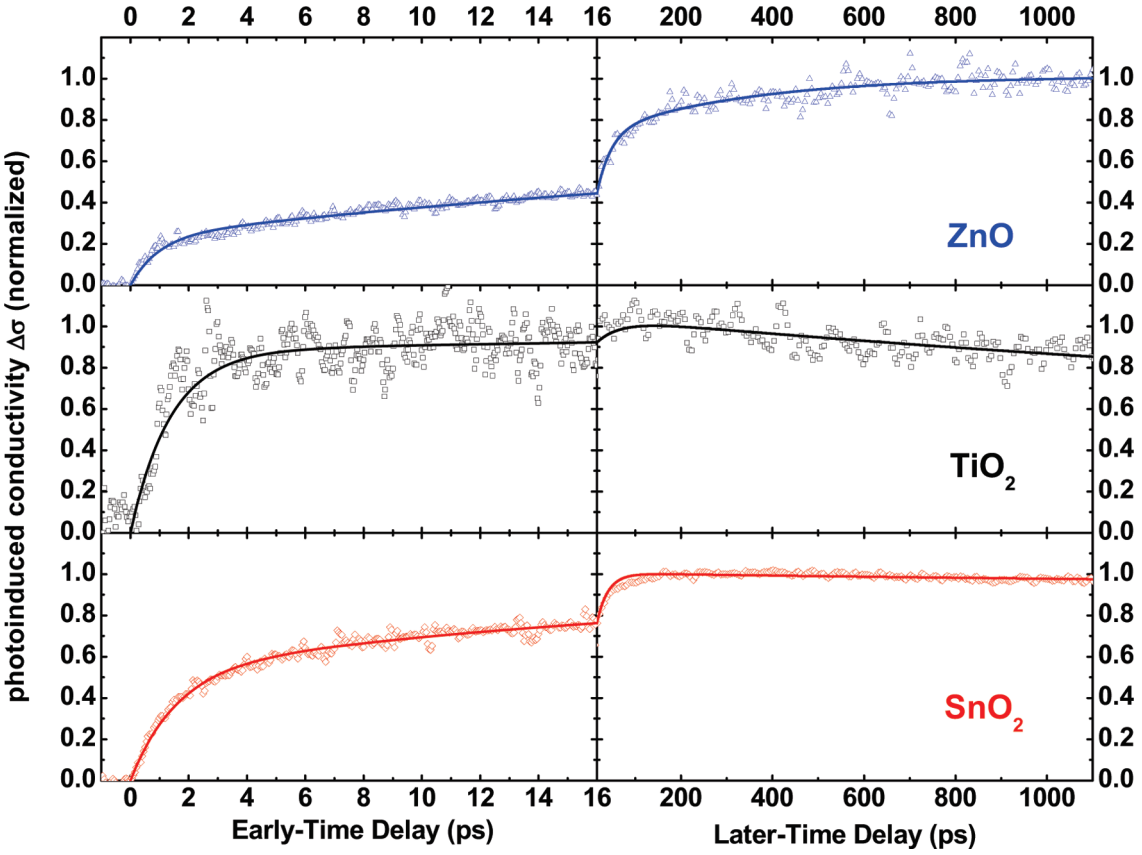

Figure 2. Early and later time photoconductivity dynamics in nanoporous ZnO, TiO_2, and SnO_2 films sensitized with Z907 dye. Early time trends (up to 16 ps) are shown on the left and later time trends (up to 1.1 ns) on the right. Dye-sensitized ZnO and SnO_2 were photoexcited at 550 nm, while TiO_2 was excited at 475 nm. Identical dynamics were observed for Z907/TiO_2 when the excitation wavelength was varied across the dye absorption spectrum between 475 and 700 nm, and a linear dependence of the photoconductivity on excitation fluence was found at these excitation densities.[16] In all three cases, incident photoexcitation fluence was $\sim 3 \times 10^{14}$ photons/cm^2, with a pulse duration of $\sim$40 fs. The curves have been normalized at the respective maxima measured for each material. Solid lines are the result of fitting the sum of three exponentials to the data, with the extracted parameters given in Table 1.

TABLE 1. Parameters Extracted from Exponential Fits to the Time-Dependent Photoconductivity Data on Sensitized Nanoporous Films of ZnO, TiO_2, and SnO_2[a]

	τ_1 (ps)	τ_2 (ps)	τ_3 (ps)	A_1	A_2	A_3
ZnO	1.0 ± 0.1	31 ± 2	335 ± 42	−0.232 ± 0.006	−0.49 ± 0.02	−0.29 ± 0.02
TiO_2	1.4 ± 0.1	51 ± 25	3000 (set)	−0.88 ± 0.02	−0.16 ± 0.02	0.61 ± 0.09
SnO_2	1.6 ± 0.1	24 ± 1	3000 (set)	−0.538 ± 0.008	−0.47 ± 0.01	0.10 ± 0.02

[a] A fitting function of $\Delta\sigma = \sum_{i=1}^{3}(A_i \exp(-t/\tau_i) - A_i)$ was used, and the resulting curves are shown in Figure 2 together with the data. Negative amplitudes A_i reflect rise components, while positive ones correspond to intensity decay.

shapes and sizes, with varying recipes, sensitized with different ruthenium dyes and with different surface conditions. As demonstrated by Ai *et al.*,[27] different film environments can change the flatband potential of the semiconductor and the reorganization energy which affects the injection rate as a result of its dependence on the interfacial proton concentration. In our study presented here, we aim to minimize such effects by preparing films in a comparable manner and sensitizing them with an identical and commonly used dye (Z907); see Materials and Methods section.

The relative rates of electron injection we observe for the three different oxides (Figure 2) are surprising at first: for ZnO, injection is slower than in TiO_2, even though both metal-oxides have almost identical interface band energetics (Figure 1). For SnO_2, we observe somewhat slower electron injection than for TiO_2, even though the CB edge of SnO_2 is more positive by $\sim$500 meV compared to TiO_2, which should increase the number of the SnO_2 acceptor states at the excited-state energy. There are, however, a number of other factors contributing to the electron transfer kinetics at the dye/metal-oxide interface. One possibility is that different amounts of dye loading for the three materials may result in slow charge injection caused by the presence of dye agglomerates on the metal-oxide film,

as proposed previously.[26,29] However, Anderson *et al.* used detailed experimental pump−probe studies carried out on N3/ZnO and N719/ZnO to show that although excess dye loading can lead to reduced overall injection yield, it does not affect the ultrafast injection rate.[21,22] Similarly, we have observed previously that the slow injection component in mesoporous TiO_2 sensitized with Z907 was unaffected by moderate changes in dye loading. We therefore assume that, given the standard optical densities for dye absorption for our samples (Figure 1), changes in dye loading are not the cause of the observed slow injection phases. As an alternative explanation, multiphasic electron injection into TiO_2[23,24] and SnO_2[17] has been attributed to different injection speeds from the singlet and triplet excited states of the dye's ruthenium complex with the femtosecond component arising from the initially excited singlet state (^{1}MLCT) and the picosecond part from the thermalized triplet ^{3}MLCT excited state. However, since we use the same dye as sensitizer for all metal-oxides, this mechanism alone cannot explain the differences in injection speeds between the three metal-oxide films.

A likely scenario is that electron injection between the three oxides is influenced by the electronic structure of the CB of the metal-oxide and the coupling of the dye molecule to the interface. The CB structure of the metal-oxides investigated differs drastically between TiO_2 on the one hand and ZnO and SnO_2 on the other hand. The effective mass of CB electrons in TiO_2 is about 5−10 m_e as opposed to a corresponding value of ∼0.3 m_e for ZnO and SnO_2.[27,30,31] Therefore, the available density of states (DOS) is almost 2 orders of magnitude higher in TiO_2 than in ZnO or SnO_2,[4,22,27,30] which should facilitate faster injection into TiO_2. An additional prerequisite for efficient electron injection is that there has to be significant extension of the dye excited-state wave function into the metal-oxide. The electron-donating π^* orbital of the carboxylated bipyridine unit on Z907 has a stronger overlap with the electron-accepting d orbitals of Ti^{4+} than with the 4s orbital of Zn^{2+}.[4,22,32] Similarly, for SnO_2, a weaker electronic overlap at the interface with N3 or N719 dyes has been suggested,[27,28] which is consistent with the slower injection we observe.

As an alternative explanation, Furube *et al.* suggested that the presence of intermediate charge transfer complexes may cause slow electron injection dynamics from sensitizers into metal-oxide films.[19,20] For ZnO nanoporous films sensitized with N3 dye, they observed that the fast (subpicosecond) generation of N3 cations following photoexcitation was not matched by the rise of the free-electron signal from ZnO, which occurred on the time scale of ∼150 ps.[19] They concluded that electron transfer from N3 to ZnO occurred *via* a two-step process involving an intermediate state between the photoexcited dye and a surface state in

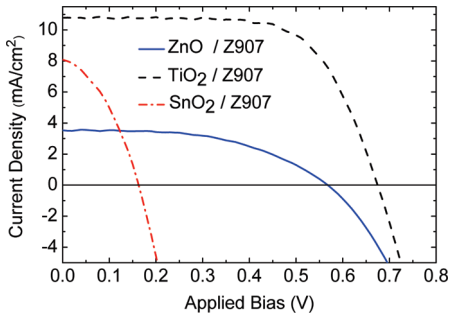

Figure 3. Current−voltage characteristics under simulated solar conditions measured for three typical liquid-electrolyte photovoltaic cells fabricated from either TiO_2, ZnO, or SnO_2 nanoporous films sensitized with Z907dye.

ZnO. For nanoporous TiO_2 sensitized with N3, on the other hand, fast electron injection was observed, suggesting that intermediate states do not play a strong role here. These measurements were corroborated later for the same systems by Neměc *et al.*, who proposed that the slow injection was the direct result of the higher static dielectric constant of TiO_2 (∼100) compared to that of ZnO (∼10), as in the former such electron−cation complex interactions may be efficiently screened.[33] We observe slow injection dynamics for both ZnO and SnO_2, both of which have similar low static dielectric constants.[34] However, the presence of multiple rise times for all three metal-oxides investigated suggests that such screening effects alone cannot be the explanation for the slow injection dynamics. All three metal-oxide systems have a fast picosecond injection component suggesting that, for all of them, fast injection pathways are available from certain sites. These findings are in agreement with further studies by Furube *et al.*[20] on nanoporous ZnO sensitized with a coumarin dye and Ai *et al.*[27] on nanoporous SnO_2 sensitized with various ruthenium dyes, for which the authors observed multiphasic electron injection into the metal-oxide with different time constants ranging from a picosecond to tens of picoseconds. To summarize these arguments, electron injection from most dye/metal-oxide systems appears to be influenced by site disorder with injection pathways and dynamics being governed by the local interface environment which may vary considerably between each dye/metal-oxide site. The particular mode of coupling of the dye to the surface and the local electronic density of states in the CB of the metal-oxide have a strong influence on electron injection dynamics, with pure energy level offsets and bulk dielectric constant playing only a secondary role.

Another relevant piece of information that can be extracted from OPTP measurements is the value of the "effective terahertz mobility" $\phi_{inj}\mu_{THz}$ of electrons within the nanoporous semiconductor film, as outlined in detail in our previous work.[16] Here, ϕ_{inj} is the charge injection efficiency per absorbed photon and μ_{THz} the

TABLE 2. Charge Injection and Mobility Parameters Determined for Nanoporous Dye-Sensitized ZnO, TiO_2, and SnO_2 Films Together with Literature Values for Some Bulk Properties (Detailed References to Each Parameter Are Given in the Main Text)

	THz effective mobility[a]	IPCE (max)[b]	photocurrent decay rate[c]	photovoltage decay rate[c]	collection efficiency	injection efficiency[d]	THz mobility[e]	bulk mobility[7,8,11]	device diffusion coefficient	device mobility[e]	static dielectric constant[3,4]
	$\phi_{inj}\mu_{THz}$, $cm^2/(V \cdot s)$	IPCE	k_{signal}, s^{-1}	k_{rec}, s^{-1}	η_{coll}	ϕ_{inj}	μ_{THz}, $cm^2/(V \cdot s)$	μ_{bulk}, $cm^2/(V \cdot s)$	D_e, cm^2/s	μ_{N-E}, $cm^2/(V \cdot s)$	$\varepsilon_{rs}\|\|,\perp$
ZnO	0.08	0.38	571.9	24.6	0.96	0.47	**0.17**	**200**	1.1×10^{-4}	**0.004**	8, 12
TiO_2	0.1	0.83	1040	20.4	0.98	1.00	**0.10**	**1**	4.3×10^{-4}	**0.017**	173, 89
SnO_2	0.8	0.63	368.2	19.6	0.95	0.79	**1.01**	**250**	7.3×10^{-5}	**0.003**	9.9, 14

[a] Value of $\phi_{inj}\mu_{THz}$ was taken from OPTP measurements of the highest $\Delta\sigma$ value; see ref 16 for details. [b] Peak spectral response in optically thick liquid-electrolyte DSCs. [c] Measurements were taken under short-circuit conditions and decay curves fitted with monoexponential functions to extract rates shown. [d] Value of ϕ_{inj} was estimated using eq 1 with light absorption within DSCs estimated to be 0.84 with deviation from unity caused by losses through absorption and reflection from FTO glass. [e] Values were determined within an experimental error of ~25%.

peak value of the film's time-dependent terahertz mobility. Being independent of sample geometry and excitation fluence, carrier mobility is a more useful material characteristic than conductivity. We have determined $\phi_{inj}\mu_{THz}$ for the three sensitized metal-oxide films from the respective measured peak photoconductivity values, incident excitation fluences, and steady-state absorption at the excitation wavelength (data shown in Figure 1b). We obtain values of $\phi_{inj}\mu_{peak}$ = 0.08 ± 0.01 $cm^2/(V \cdot s)$ for nanostructured ZnO, 0.1 ± 0.03 $cm^2/(V \cdot s)$ for TiO_2, and 0.8 ± 0.14 $cm^2/(V \cdot s)$ for SnO_2.

In order to extract the actual mobility μ_{THz} from these values, we determined ϕ_{inj} from measurements on liquid-electrolyte DSCs based on the three metal-oxides films. Figure 3 shows the $J-V$ curves measured for three typical devices. As expected, solar cells based on SnO_2 show a markedly lower open-circuit voltage than those based on TiO_2 or ZnO[35,36] predominantly as a result of the differing CB levels. However, recombination losses at open-circuit also contribute to the lowering of the open-circuit voltage for bare SnO_2. We determined the incident photon-to-electron conversion efficiency (IPCE) for the devices, which is related to the charge injection efficiency, ϕ_{inj} through

$$\text{IPCE} = \text{LHE} \times \phi_{inj} \times \eta_{coll} \quad (1)$$

Here, LHE is the light-harvesting efficiency of the device as determined from absorption measurements, and η_{coll} is the charge collection efficiency which we established from small perturbation transient photovoltage and photocurrent decay measurements. The values determined for IPCE, LHE, and η_{coll} are shown in Table 2 with full details of the measurements and calculation methods provided in the Materials and Methods section.

Table 2 lists the average values of ϕ_{inj} determined for the three different oxides. For the case of Z907/TiO_2, a charge injection efficiency of 100% indicates that this dye−semiconductor system is highly optimized, in comparison to the other two materials. Interestingly, ZnO performs worse (ϕ_{inj} = 0.47) than SnO_2 (ϕ_{inj} = 0.79), in agreement with our observations of delayed charge injection components (Figure 2). Our combination of OPTP with device measurements suggests that the more pronounced a slow component is in the electron injection dynamics for the metal-oxide films, the lower the overall charge injection efficiency of the solar cell will be. Better matched dyes thus need to be designed specifically for ZnO and SnO_2 that allow near-unity charge injection from the dye at rates significantly faster than the dye's excited-state lifetime. It is important to note that the charge collection efficiency at short-circuit for devices fabricated from all three oxides is higher than 0.95, consistent with the change in the injection efficiency being the performance-limiting factor.

Using the values obtained for ϕ_{inj}, we thus extract the terahertz peak mobility μ_{THz} of the films as 0.17 ± 0.04 $cm^2/(V \cdot s)$ for ZnO, 0.10 ± 0.03 $cm^2/(V \cdot s)$ for TiO_2, and 1.01 ± 0.20 $cm^2/(V \cdot s)$ for SnO_2. It should be stressed that these results reflect the terahertz conductivity conditions within the first nanosecond after electron injection into the metal-oxide films, while in the longer term, the conductivity is likely to be lowered by charge trapping and surface scattering events.[37] It is therefore useful to compare μ_{THz} with the electron mobility obtained for devices incorporating the nanoporous films. For this purpose, we conducted transient voltage and current decay measurements that yield the current collection rate k_{trans} in the photovoltaic cells fabricated from the dye-sensitized films. The device mobility was then calculated using the Nernst–Einstein relation:[38]

$$\mu_{NE} = \frac{eD_e}{k_B T} \text{ and } D_e = \frac{d^2 k_{trans}}{2.35} \quad (2)$$

where D_e is the effective electron diffusion coefficient and d is the film thickness. A third measure of mobility against which these results may be compared are the values determined by others for bulk single crystals of the three metal-oxides. In single crystals, surface scattering and trapping are likely to be minimized and the electron mobility determined can therefore be seen as an upper limit of what may be achieved in the nanoporous film. Table 2 lists bulk mobility values (μ_{bulk}) found in the literature for room-temperature Hall measurements on single crystals of ZnO,[7] TiO_2,[11] and SnO_2,[8] together with those we extracted from terahertz (μ_{THz}) and device (μ_{NE}) measurements.

A number of interesting observations can be made by comparing these three measures of electron mobility for the three different metal-oxides. First, a comparison between μ_{THz} and μ_{bulk} reveals that while for TiO_2 the terahertz mobility is within an order of magnitude of the bulk mobility value, for ZnO and SnO_2, this discrepancy widens to 2–3 orders of magnitude. Hendry *et al.* previously measured an early time terahertz charge mobility for unsensitized porous TiO_2 films of $10^{-2} cm^2/(V \cdot s)$, that is, 2 orders of magnitude below the bulk crystal mobility.[37] They attributed this discrepancy to the nanoporous nature of the films in which dipoles induced in the TiO_2 particles with high dielectric constant screen the applied electric field, thus resulting in the flux density to be higher in the medium surrounding the particle than within. As a consequence, the mobility of the nanoporous TiO_2 film is likely to be intrinsically lower than that of bulk, by a factor which may be approximated from Maxwell–Garnett (MG) theory.[37] The terahertz mobility value we determine for nanoporous TiO_2 is 1 order of magnitude higher than that found by Hendry *et al.*, which may be the consequence of the nanoparticles being in our case embedded in a medium of higher dielectric constant (the sensitizer) and perhaps different fabrication protocols. We therefore conclude that for sensitized nanoporous TiO_2 films a slight (factor ~0.1) reduction of the achievable mobility below that of single crystals may have to be accepted as a result of MG effects. However, for ZnO and SnO_2, this situation is markedly different: Table 2 lists values for the static dielectric constant ε_{rs}, which approximate those at terahertz frequencies, for the three different metal-oxides as found in ref 34. For ZnO and SnO_2, the dielectric constant is over an order of magnitude lower than that for TiO_2, and therefore MG effects are likely to be much less significant for these two metal-oxide nanoporous materials. Given that for TiO_2 we find MG effects to lead to a mobility reduction of at most a factor 0.1, these effects are likely to be insignificant for ZnO and SnO_2. The observed terahertz mobility reduction for ZnO and SnO_2 nanoporous films of over 2 orders of magnitude below the corresponding single-crystal electron mobilities is therefore surprising and points toward electron mobilities on the nanometer scale that are significantly below what should in theory be achievable.

A second useful comparison to make is between the electron mobility found in complete devices and that found in bulk crystals. The values given in Table 2 show that there is little positive correlation between μ_{NE} and μ_{bulk}; in fact, TiO_2 exhibits the highest device mobility (0.017 $cm^2\ V^{-1}\ s^{-1}$) but lowest bulk crystal mobility (1 $cm^2\ V^{-1}\ s^{-1}$), while SnO_2 gives lowest device mobility (0.003 $cm^2\ V^{-1}\ s^{-1}$) at highest bulk crystal mobility (250 $cm^2\ V^{-1}\ s^{-1}$). The electron mobility measured for the nanoporous thin-film devices (μ_{NE}) reflects the time-averaged mobility throughout the film and is therefore significantly affected by *interparticle* transfer, surface scattering, and trapping. In contrast, the terahertz mobility (μ_{THz}) indicates conditions within the first nanosecond after electron injection into the metal-oxide films and is thus strongly affected by short-distance electron transport and scattering. Overall, we note that while ZnO and SnO_2 exhibit bulk crystal mobilities over 2 orders of magnitudes higher than that for TiO_2, the early time, short-distance terahertz mobilities are similar for the three metal-oxide nanoporous films, and the corresponding device mobilities are almost an order of magnitude lower for ZnO and SnO_2 than for TiO_2. Taken together, these comparisons show that while TiO_2 nanoporous films are reaching near optimum results for a porous effective medium of high dielectric constant, the standard ZnO and SnO_2 nanoporous films investigated here are still 4–5 orders of magnitude away from what could theoretically be achieved in terms of electron mobility. Our findings on ZnO are in agreement with those of Baxter *et al.*, showing that a wide variation in terahertz mobility values can be found for samples

fabricated from ZnO films, nanowires, and nanoparticles, with the lowest mobility measured in the nanoparticles.[39] Improving both nano- and micrometer scale conduction pathways in ZnO and SnO_2 should therefore allow significant advances to be made in photovoltaic device performance. Even though our study demonstrates that the charge collection efficiency at short-circuit is high for all three oxides, under forward bias working conditions, the charge collection efficiency reduces considerably[40] and almost by definition is close to zero at open-circuit. Therefore, enhancing the charge transport in the oxide will significantly improve the photocurrent under working conditions and hence the fill factor and efficiency for solar cells based on nanostructured ZnO and SnO_2.

CONCLUSION

In conclusion, we have conducted a comparative study of electron injection and mobility in nanoporous films of three different metal-oxides, TiO_2, ZnO, and SnO_2 sensitized with Z907 dye. By measuring the terahertz conductivity in the metal-oxide as a function of time after photoexcitation of the dye, we were able to examine the dynamics of electron injection from the dye into the metal-oxide. We find significant slow injection components lasting predominantly over a few hundred picoseconds after excitation for ZnO and tens of picoseconds for SnO_2. For TiO_2, on the other hand, such delayed electron injection plays a minor role and mostly features within the first few picoseconds. These results correlate well with the overall electron injection efficiencies we determined from photovoltaic cells fabricated from identical nanoporous films of the three oxides. Such slow injection components thus allow effective competition between charge injection and excitonic recombination on the sensitizer and must be overcome for further device efficiency gains. The extent to which slow injection components are present was found to be largely independent of the energetic positioning of the metal-oxide conduction and valence bands. We therefore conclude that other factors such as the density of states for the bands and the local binding and orbital overlap of the sensitizer on the metal-oxide surface are more important. The design of dyes that are better matched and attached to the electron acceptor should hence lead to improvements in charge generation efficiencies for ZnO and SnO_2.

In addition, we have used a combination of terahertz conductivity and transient device photocurrent measurements in order to determine the electron mobility in the nanoporous metal-oxide films both at early time after injection (μ_{THz}) and for the time-averaged long-distance motion of electrons through the film (μ_{NE}). Comparing these results with established values for the Hall mobility in single-crystal of the three metal-oxides (μ_{bulk}), we find that while ZnO and SnO_2 have μ_{bulk} values 2−3 orders of magnitude higher than that for TiO_2, the values obtained for the early time μ_{THz} are identical within an order of magnitude for the three metal-oxides. Furthermore, device mobility values μ_{NE} for the three different materials show the reverse trend from those for μ_{bulk}: here, TiO_2 yields μ_{NE} significantly higher than those obtained for either ZnO or SnO_2 nanoporous films. These results show that the early time, short distance, and the interparticle electron motion in ZnO or SnO_2 are far from optimized. We conclude that while electron mobility values for devices incorporating TiO_2 nanoporous films are now approaching optimum theoretical values, those for ZnO or SnO_2 still offer room for improvement of several orders of magnitude.

MATERIALS AND METHODS

Preparation of Dye-Sensitized Metal-Oxide Films. ZnO paste was prepared using ZnO nanopowder purchased from Sigma Aldrich (544906, <100 nm size). The powder was ground with ethanol, dissolved in terpineol, and ethyl cellulose and sonicated to achieve a well-dispersed paste. The nanoparticle concentration was adjusted depending on the method of film preparation, spin-coating, or screen-printing. TiO_2 paste (20 nm particle diameter) was purchased from Dyesol (18NR-T) and thinned with ethanol as required. The SnO_2 paste was prepared in Michael Grätzel's group at EPFL using an aqueous colloidal suspension of SnO_2 nanoparticles (10 nm wide, 20 nm long), using the recipe detailed in ref 36. Following deposition into thin nanoporous films, sensitization was carried out by immersing them in 0.3 mM Z907 dye solution in acetonitrile/*tert*-butanol (1:1 vol %) for 14 h at room temperature. The films were then rinsed in acetonitrile to remove any dye not physically adsorbed on the semiconductor surface. Z907 is a well-studied amphiphilic ruthenium complex, *cis*-bis(isothiocyanato)(2,2′-bipyridyl-4,4′-dicarboxylato)(4,4′-dinonyl-2′-bipyridyl)ruthenium(II), which yields high performance DSCs.[16,41]

Samples for Terahertz Study. In all cases, the paste was spin-coated on z-cut quartz substrates, and the films were sintered slowly in air at 500 °C after which sensitization was carried out as described above. This process yielded film thicknesses of 0.6 μm for ZnO, 3 μm for TiO_2, and 1 μm for SnO_2 films, as measured with a Veeco DekTak 150 surface profiler. Typical steady-state absorption spectra measured using a Cary 300 spectrophotometer integrated with a "Labsphere" integrating sphere are shown in Figure 1b. Measurements were carried out using the protocol outlined in our previous work.[36] Minimum exposure of the dyed samples to UV light was ensured to prevent the dye from being oxidized or degraded.

Optical Pump Terahertz Probe (OPTP) Spectroscopy. Details about the OPTP setup used in this study can be found in ref 16. Dye-sensitized films were photoexcited using 40 fs duration pulses at 550 nm (ZnO and SnO_2) or 475 nm (TiO_2) wavelength. Photon absorption causes electrons to be excited into the dye LUMO states, which are subsequently injected into the semiconductor

conduction band (CB) where they are relatively free to move. The photoconductivity induced in the sample is then probed using picosecond duration terahertz pulses generated using optical rectification in a ZnTe crystal with 40 fs 800 nm pulses.[42] Part of these terahertz pulses are absorbed by the mobile charge carriers present in the sample. The remaining transmitted terahertz signal is then measured using a double lock-in technique and provides a direct measurement of the sample carrier conductivity, as discussed in ref 16.

All pump−probe experiments in this study were performed at room temperature and under vacuum ($<10^{-3}$ mbar pressure). The incident pump fluence was kept low in order to avoid charge−charge interactions,[43] typically at about $10^{13}-10^{14}$ photons/cm^2 per pulse. This is equivalent to the solar energy incident on a DSC under standard operating conditions. Sample integrity was checked before and after the experiments by measuring the steady-state absorption spectrum to verify negligible sample degradation.

Device Preparation. A compact layer of the relevant metal-oxide (*e.g.*, SnO_2 compact layer for SnO_2 devices) was coated using spray pyrolysis on FTO glass (15 Ω/□, Pilkington) at 450 °C to achieve a thickness of ∼100 nm. For SnO_2, butyltin trichloride (95%, Sigma Aldrich) at a 250 mM concentration in anhydrous ethanol was used; for TiO_2, titanium diisopropoxide bis-(acetylacetonate) (Sigma Aldrich, 75% by weight in isopropyl alcohol) at a 250 mM concentration in anhydrous ethanol was used; and for ZnO, zinc acetate dihydrate (99.999%, Sigma Aldrich) at 100 mM concentration in anhydrous methanol was used. The ZnO, TiO_2, and SnO_2 pastes were subsequently screen-printed on the substrates and slowly sintered with a slow ramp up to 500 °C, resulting in ≥7 μm thick films. The films were subsequently sensitized with Z907 dye as detailed above resulting in optical densities (OD) at peak absorption of OD > 2. Counter electrodes were prepared by coating FTO glass with 0.05 M hexachloroplatinic acid in anhydrous isopropyl alcohol at 400 °C for 15 min. This FTO glass was then assembled in a sandwich-type configuration with the dye-sensitized metal-oxide-coated FTO glass, using a "hotmelt" 25 μm thick Surlyn spacer (Dupont) at 200 °C to seal the working and counter electrodes together. A drop of "robust" electrolyte (0.8 M PMII, 0.15 M iodine, 0.1 M GuNCS, and 0.5 M NMBI in 3-methoxypropionitrile) was injected into the interelectrode space from a predrilled hole in the counter electrode *via* vacuum backfilling.[44] The hole was then sealed with a Bynel sheet (Dupont) and a thin glass cover slide by locally heating the hole to 450 °C with a soldering iron.

Current Voltage Measurements. AM1.5 light at 100 mW/cm^2 was generated using an ABET solar simulator calibrated using an NREL calibrated silicon reference cell with a KG5 filter to minimize spectral mismatch. *J*−*V* curves were measured with a Keithley 2400 unit. The solar cells were masked with a metal aperture to define the active area and to eliminate any edge effects.

Incident Photon-to-Electron Conversion Efficiency (IPCE) Measurements. IPCE spectra were measured on thick electrolyte DSC devices across the visible spectrum under short-circuit conditions. The IPCE spectral response was taken under monochromatic light with an intensity of approximately 1 mW cm^{-2} and the response calibrated with a silicon reference diode. Overall low-light intensities were used because it is difficult in practice to optically bias the cells under AM1.5 sun light while measuring the spectral response because the response speed of the DSCs is often too slow for conventional choppers.[45] The peak spectral response was corrected by integrating the measured IPCE spectra over the AM1.5 solar spectra at 100 mW cm^{-2}, such that the integrated short-circuit photocurrent was in close agreement with the maximum photocurrent value measured in the *J*−*V* curves under simulated solar conditions.

Determination of the Light Harvesting Efficiency (LHE). LHE is a measure of the fraction of incident photons successfully absorbed within the active layers in the DSC. All nanoporous layers (ZnO, TiO_2, and SnO_2) in our devices were thick enough (≥7 μm) to be fully absorbing. Hence, the main losses were due to reflection and absorption in the light-facing FTO glass, measured to be 12.3 and 3.6%, respectively, at 550 nm using the integrating sphere accessory of a spectrophotometer. The LHE was thus determined to be 84% for all three sets of devices.

Small Perturbation Transient Photovoltage and Photocurrent Decay Measurements. Measurements were carried out on the liquid electrolyte DSCs in order to determine η_{coll} using the setup described in ref 46. The sample under measurement was biased with a white light equivalent to 100 mW/cm^2 intensity and perturbed with a red light pulsed diode. The perturbation was kept small enough to ensure that the voltage decay dynamics were monoexponential. All data were collected under equivalent to short-circuit conditions, that is, holding the bias at 0 V for the photocurrent transients (potentiostatic mode) and holding the current J_{sc} generated by the white-light bias constant for the voltage perturbation measurements (galvinostatic mode). In the latter case, because the current sourced through the device is forced to be constant, any extra charges generated due to the perturbation pulse must therefore recombine over time since the extra charge cannot leave the device. These decay traces therefore yield the recombination rate, k_{rec}. The decay usually happens on a relatively long time scale of tens to hundreds of milliseconds because the charge density in the film at short-circuit is very low in comparison to that under open-circuit conditions. On the other hand, in the case of current decay measurement under short-circuit condition, charge transport occurs in parallel with recombination. The decay rate of the signal at 0 V (k_{signal}) therefore is a combination of k_{rec} and the transport rate, k_{trans}, as $k_{signal} = k_{trans} + k_{rec}$. The charge collection efficiency was then estimated from the two measurements as

$$\eta_{coll} = \frac{k_{trans}}{k_{signal}} \quad (3)$$

Acknowledgment. This work was funded by the Engineering and Physical Sciences Research Council (UK). We thank Pascal Comte and Michael Graetzel from the École Polytechnique Fédérale de Lausanne for providing the SnO_2 nanoparticle paste.

REFERENCES AND NOTES

1. Green, M. A.; Emery, K.; Hishikawa, Y.; Warta, W. Solar Cell Efficiency Tables (Version 35). *Prog. Photovoltaics* **2010**, *18*, 144–150.
2. Grätzel, M. Photoelectrochemical Cells. *Nature* **2001**, *414*, 338.
3. Katoh, R.; Furube, A.; Yoshihara, T.; Hara, K.; Fujihashi, G.; Takano, S.; Murata, S.; Arakawa, H.; Tachiya, M. Efficiencies of Electron Injection from Excited N3 Dye into Nanocrystalline Semiconductor (ZrO_2, TiO_2, ZnO, Nb_2O_5, SnO_2, In_2O_3) Films. *J. Phys. Chem. B* **2004**, *108*, 4818–4822.
4. Asbury, J. B.; Hao, E.; Wang, Y. Q.; Ghosh, H. N.; Lian, T. Q. Ultrafast Electron Transfer Dynamics from Molecular Adsorbates to Semiconductor Nanocrystalline Thin Films. *J. Phys. Chem. B* **2001**, *105*, 4545–4557.
5. Fessenden, R. W.; Kamat, P. V. Rate Constants for Charge Injection from Excited Sensitizer into SnO_2, ZnO, and TiO_2 Semiconductor Nanocrystallites. *J. Phys. Chem.* **1995**, *99*, 12902–12906.
6. Fukai, Y.; Kondo, Y.; Mori, S.; Suzuki, E. Highly Efficient Dye-Sensitized SnO_2 Solar Cells Having Sufficient Electron Diffusion Length. *Electrochem. Commun.* **2007**, *9*, 1439–1443.
7. Look, D. C.; Reynolds, D. C.; Sizelove, J. R.; Jones, R. L.; Litton, C. W.; Cantwell, G.; Harsch, W. C. Electrical Properties of Bulk ZnO. *Solid State Commun.* **1998**, *105*, 399–401.
8. Jarzebski, Z. M.; Marton, J. P. Physical Properties of SnO_2 Materials. II. Electrical Properties. *J. Electrochem. Soc.* **1976**, *123*, 299C–310C.
9. Jousse, D.; Constantino, C.; Chambouleyron, I. Highly Conductive and Transparent Amorphous Tin Oxide. *J. Appl. Phys.* **1983**, *54*, 431–434.
10. Shanthi, E.; Dutta, V.; Banerjee, A.; Chopra, K. L. Electrical and Optical Properties of Undoped and Antimony-Doped Tin Oxide-Films. *J. Appl. Phys.* **1980**, *51*, 6243–6251.

11. Yagi, E.; Hasiguti, R. R.; Aono, M. Electronic Conduction above 4 K of Slightly Reduced Oxygen-Deficient Rutile TiO_{2-x}. *Phys. Rev. B* **1996**, *54*, 7945–7956.
12. Özgür, U.; Alivov, Y. I.; Liu, C.; Teke, A.; Reshchikov, M. A.; Doğan, S.; Avrutin, V.; Cho, S. J.; Morkoç, H. A Comprehensive Review of ZnO Materials and Devices. *J. Appl. Phys.* **2005**, *98*, 041301.
13. Zarzebski, Z. M.; Marton, J. P. Physical Properties of SnO_2 Materials. 3. Optical Properties. *J. Electrochem. Soc.* **1976**, *123*, C333–C346.
14. Parkinson, P.; Lloyd-Hughes, J.; Johnston, M. B.; Herz, L. M. Efficient Generation of Charges *via* Below-Gap Photoexcitation of Polymer–Fullerene Blend Films Investigated by Terahertz Spectroscopy. *Phys. Rev. B* **2008**, *78*, 115321.
15. Parkinson, P.; Joyce, H. J.; Gao, Q.; Tan, H. H.; Zhang, X.; Zou, J.; Jagadish, C.; Herz, L. M.; Johnston, M. B. Carrier Lifetime and Mobility Enhancement in Nearly Defect-Free Core–Shell Nanowires Measured Using Time-Resolved Terahertz Spectroscopy. *Nano Lett.* **2009**, *9*, 3349–3353.
16. Tiwana, P.; Parkinson, P.; Johnston, M. B.; Snaith, H. J.; Herz, L. M. Ultrafast Terahertz Conductivity Dynamics in Mesoporous TiO_2: Influence of Dye Sensitization and Surface Treatment in Solid-State Dye-Sensitized Solar Cells. *J. Phys. Chem. C* **2010**, *114*, 1365–1371.
17. Benko, G.; Myllyperkio, P.; Pan, J.; Yartsev, A. P.; Sundström, V. Photoinduced Electron Injection from Ru(dcbpy)(2)(NCS)(2) to SnO_2 and TiO_2 Nanocrystalline Films. *J. Am. Chem. Soc.* **2003**, *125*, 1118–1119.
18. Wang, P.; Wenger, B.; Humphry-baker, R.; Moser, J.-E.; Teuscher, J.; Kantlehner, W.; Mezger, J.; Stoyanov, E. V.; Zakeeruddin, S. M.; Grätzel, M. Charge Separation and Efficient Light Energy Conversion in Sensitized Mesoscopic Solar Cells Based on Binary Ionic Liquids. *J. Am. Chem. Soc.* **2005**, *127*, 6850–6856.
19. Furube, A.; Katoh, R.; Hara, K.; Murata, S.; Arakawa, H.; Tachiya, M. Ultrafast Stepwise Electron Injection from Photoexcited Ru-Complex into Nanocrystalline ZnO Film *via* Intermediates at the Surface. *J. Phys. Chem. B* **2003**, *107*, 4162–4166.
20. Furube, A.; Katoh, R.; Yoshihara, T.; Hara, K.; Murata, S.; Arakawa, H.; Tachiya, M. Ultrafast Direct and Indirect Electron-Injection Processes in a Photoexcited Dye-Sensitized Nanocrystalline Zinc Oxide Film: the Importance of Exciplex Intermediates at the Surface. *J. Phys. Chem. B* **2004**, *108*, 12583–12592.
21. Asbury, J. B.; Wang, Y. Q.; Lian, T. Q. Multiple-exponential Electron Injection in Ru(dcbpy)(2)(SCN)(2) Sensitized ZnO Nanocrystalline Thin Films. *J. Phys. Chem. B* **1999**, *103*, 6643–6647.
22. Anderson, N. A.; Ai, X.; Lian, T. Q. Electron Injection Dynamics from Ru Polypyridyl Complexes to ZnO Nanocrystalline Thin Films. *J. Phys. Chem. B* **2003**, *107*, 14414–14421.
23. Benko, G.; Kallioinen, J.; Korppi-tommola, J. E. I.; Yartsev, A. P.; Sundström, V. Photoinduced Ultrafast Dye-to-Semiconductor Electron Injection from Nonthermalized and Thermalized Donor States. *J. Am. Chem. Soc.* **2002**, *124*, 489–493.
24. Benko, G.; Kallioinen, J.; Myllyperkio, P.; Trif, F.; Korppi-tommola, J. E. I.; Yartsev, A. P.; Sundström, V. Interligand Electron Transfer Determines Triplet Excited State Electron Injection in RuN3-Sensitized TiO_2 Films. *J. Phys. Chem. B* **2004**, *108*, 2862–2867.
25. Tachibana, Y.; Nazeeruddin, M. K.; Grätzel, M.; Klug, D. R.; Durrant, J. R. Electron Injection Kinetics for the Nanocrystalline TiO_2 Films Sensitised with the Dye (Bu4N)(2)Ru(dcbpyH)(2)(NCS)(2). *Chem. Phys.* **2002**, *285*, 127–132.
26. Wenger, B.; Grätzel, M.; Moser, J.-E. Rationale for Kinetic Heterogeneity of Ultrafast Light-Induced Electron Transfer from Ru(II) Complex Sensitizers to Nanocrystalline TiO_2. *J. Am. Chem. Soc.* **2005**, *127*, 12150.
27. Ai, X.; Anderson, N. A.; Guo, J. C.; Lian, T. Q. Electron Injection Dynamics of Ru Polypyridyl Complexes on SnO_2 Nanocrystalline Thin Films. *J. Phys. Chem. B* **2005**, *109*, 7088–7094.
28. Bauer, C.; Boschloo, G.; Mukhtar, E.; Hagfeldt, A. Ultrafast Studies of Electron Injection in Ru Dye Sensitized SnO_2 Nanocrystalline Thin Film. *Int. J. Photoenergy* **2002**, *4*, 17–20.
29. Bauer, C.; Boschloo, G.; Mukhtar, E.; Hagfeldt, A. Electron Injection and Recombination in Ru(dcbpy)(2)(NCS)2 Sensitized Nanostructured ZnO. *J. Phys. Chem. B* **2001**, *105*, 5585–5588.
30. Enright, B.; Fitzmaurice, D. Spectroscopic Determination of Electron and Hole Effective Masses in a Nanocrystalline Semiconductor Film. *J. Phys. Chem.* **1996**, *100*, 1027–1035.
31. Robertson, J. Electronic Structure of SnO_2, GeO_2, PbO_2, TeO_2 and MgF_2. *J. Phys. C: Solid State Phys.* **1979**, *12*, 4767–4776.
32. Petersson, A.; Ratner, M.; Karlsson, H. O. Injection Time in the Metaloxide–Molecule Interface Calculated within the Tight-Binding Model. *J. Phys. Chem. B* **2000**, *104*, 8498–8502.
33. Němec, H.; Rochford, J.; Taratula, O.; Galoppini, E.; Kužel, P.; Polìvka, T.; Yartsev, A.; Sundström, V. Influence of the Electron–Cation Interaction on Electron Mobility in Dye-Sensitized ZnO and TiO_2 Nanocrystals: A Study Using Ultrafast Terahertz Spectroscopy. *Phys. Rev. Lett.* **2010**, *104*, 197401.
34. Tsuda, N.; Nasu, K.; Yanase, A.; Siratori, K. *Electronic Conduction in Oxides*; Springer-Verlag: Berlin, 1990.
35. Tennakone, K.; Bandara, J.; Bandaranayake, P. K. M.; Kumara, G. R. A.; Konno, A. Enhanced Efficiency of a Dye-Sensitized Solar Cell Made from MgO-Coated Nanocrystalline SnO_2. *Jpn. J. Appl. Phys. Part 2* **2001**, *40*, L732–L734.
36. Snaith, H. J.; Ducati, C. SnO_2-Based Dye-Sensitized Hybrid Solar Cells Exhibiting near Unity Absorbed Photon-to-Electron Conversion Efficiency. *Nano Lett.* **2010**, *10*, 1259–1265.
37. Hendry, E.; Koeberg, M.; O'Regan, B.; Bonn, M. Local Field Effects on Electron Transport in Nanostructured TiO_2 Revealed by Terahertz Spectroscopy. *Nano Lett.* **2006**, *6*, 755.
38. Snaith, H. J.; Grätzel, M. Electron and Hole Transport Through Mesoporous TiO_2 Infiltrated with Spiro-MeOTAD. *Adv. Mater.* **2007**, *19*, 3643.
39. Baxter, J. B.; Schmuttenmaer, C. A. Conductivity of ZnO Nanowires, Nanoparticles, and Thin Films Using Time-Resolved Terahertz Spectroscopy. *J. Phys. Chem. B* **2006**, *110*, 25229–25239.
40. Cai, N.; Moon, S.-M.; L Cevey-Ha, L.; Moehl, T.; Humphry-Baker, R.; Wang, P.; Zakeeruddin, S. M.; Grätzel, M. An Organic D-π-A Dye for Record Efficiency Solid-State Sensitized Heterojunction Solar Cells. *Nano Lett.* **2011**, *11*, 1452.
41. Snaith, H. J.; Zakeeruddin, S. M.; Schmidt-Mende, L.; Klein, C.; Grätzel, M. Ion-Coordinating Sensitizer in Solid-State Hybrid Solar Cells. *Angew. Chem., Int. Ed.* **2005**, *44*, 6413.
42. Beard, M. C.; Turner, G. M.; Schmuttenmaer, C. A. Terahertz Spectroscopy. *J. Phys. Chem. B* **2002**, *106*, 7146.
43. Hendry, E.; Koeberg, M.; Pijpers, J.; Bonn, M. Reduction of Carrier Mobility in Semiconductors Caused by Charge–Charge Interactions. *Phys. Rev. B* **2007**, *75*, 233202.
44. Kuang, D. B.; Ito, S.; Wenger, B.; Klein, C.; Moser, J.-E.; Humphry-baker, R.; Zakeeruddin, S. M.; Grätzel, M. High Molar Extinction Coefficient Heteroleptic Ruthenium Complexes for Thin Film Dye-Sensitized Solar Cells. *J. Am. Chem. Soc.* **2006**, *128*, 4146–4154.
45. Sommeling, P. M.; Rieffe, H. C.; van Roosmalen, J. A. M.; Schönecker, A.; Kroon, J. M.; Wienke, J. A.; Hinsch, A. Spectral Response and *IV*-Characterization of Dye-Sensitized Nanocrystalline TiO_2 Solar Cells. *Sol. Energy Mater. Sol. Cells* **2000**, *62*, 399.
46. Snaith, H. J.; Humphry-baker, R.; Chen, P.; Cesar, I.; Zakeeruddin, S. M.; Grätzel, M. Charge Collection and Pore Filling in Solid-State Dye-Sensitized Solar Cells. *Nanotechnology* **2008**, *19*, 424003.